

Testing the BH* Model: a UV-to-Optical Spectral Fitting of *The Cliff*

Rosa M. Mérida^{1*}, Marcin Sawicki¹, Gaia Gaspar^{1,2}, Chris J. Willott³, and Kartheik G. Iyer⁴

¹ Institute for Computational Astrophysics and Department of Astronomy and Physics, Saint Mary's University, 923 Robie Street, Halifax, NS B3H 3C3, Canada

² Observatorio Astronómico de Córdoba, Universidad Nacional de Córdoba, Laprida 854, X5000, Córdoba, Argentina

³ National Research Council of Canada, Herzberg Astronomy & Astrophysics Research Centre, 5071 West Saanich Road, Victoria, BC, V9E 2E7, Canada

⁴ Columbia Astrophysics Laboratory, Columbia University, 550 West 120th Street, New York, NY 10027, USA

Received September 30, 20XX

ABSTRACT

In the black hole star (BH*) framework, the characteristic “V”-shaped spectral energy distribution of Little Red Dots (LRDs) is produced by an accreting BH embedded in a dense neutral-gas envelope with a near-unity covering factor. This envelope reprocesses the radiation and emits as a $\sim 5,000$ K blackbody, producing the optical continuum in LRDs. Meanwhile, the ultraviolet (UV) is powered by a low-mass, dust-free, metal-poor host. The BH* scenario is promising, but it has yet to undergo detailed testing; conducting a self-consistent UV-to-optical spectral-fitting analysis of LRDs would provide a robust assessment of the model. In this work, we test the BH* scenario by fitting the full JWST/NIRSpec PRISM spectrum of *The Cliff* ($z_{\text{spec}} = 3.55$), an LRD that played a pivotal role in the development of the BH* model. We find that a Bagnpipes fit that allows stellar, nebular, active galactic nucleus (AGN), and blackbody components naturally yields a BH*-like solution for *The Cliff*, even with broad priors. Our method allows us to characterize its host, despite remaining unresolved in JWST imaging. From the continuum, we infer the host to be low-mass ($\log M_*/M_\odot \sim 7.7$), star-forming, metal-poor, affected by **non-negligible dust attenuation** ($A_V \sim 0.5$ mag) acting on both stellar and nebular components. Larger stellar masses (up to $\log M_*/M_\odot \sim 8.1$) and attenuations (up to $A_V \sim 1$ mag) are obtained depending on the assumed dust attenuation law. **Modest AGN UV leakage** is consistently allowed—and sometimes preferred—by the code, but remains weak and not robustly constrained, with both AGN+host and host-dominated UV scenarios yielding statistically equivalent fits. The star formation history of the host is relatively smooth, with the galaxy already assembling $\log M_*/M_\odot \sim 7$ about 200 Myr before $z_{\text{spec}} = 3.55$. The BH-to- M_* ratio consistently exceeds the values expected from BH–host scaling relations, especially at recent times. This tension may indicate either inaccurate estimates of the BH properties or non-coeval BH–host evolution in this LRD.

Key words. Galaxies: active – high-redshift – structure – evolution

1. Introduction

Thanks to an increasing amount of multi-band photometric and spectroscopic data spanning from X-ray to radio wavelengths, our view of the so-called Little Red Dots (LRDs; Labbé et al. 2023, Barro et al. 2024, Greene et al. 2024, Matthee et al. 2024) has become much clearer in recent years. A broad set of observational properties has now been established for LRDs, including (i) their high- z nature (i.e., their number density drops 1 – 2 dex from $z \sim 4$ to $z \sim 2$; Kocevski et al. 2025, Inayoshi 2025, Ma et al. 2026, Zhuang et al. 2026); (ii) the absence of X-ray, submillimeter, and radio emission (e.g., Labbé et al. 2023, Ananna et al. 2024, Casey et al. 2024, Maiolino et al. 2024, Labbe et al. 2025, Perger et al. 2025, Setton et al. 2025); (iii) their broad Balmer and Paschen lines; (iv) their characteristic “V”-shaped spectral energy distributions (SEDs); (v) compactness; and (vi) lack of variability (e.g., Kokubo & Harikane 2025, Furtak et al. 2025, Zhang et al. 2025).

More recently, a new wave of discoveries has further complicated this landscape. These include (vii) the report of extremely large Balmer breaks, arguably not stellar, in some LRDs (e.g., de Graaff et al. 2025c, Naidu et al. 2025); (viii) the presence of Balmer-line absorption in many LRDs (e.g., Juodžbalis et al. 2024, D’Eugenio et al. 2025); (ix) the discovery of potential lo-

cal analogs (e.g., Lin et al. 2025, 2026a, Ji et al. 2026); or (x) the detection of high-ionization emission lines in some LRDs (e.g., Labbe et al. 2024, Akins et al. 2025a, Torralba et al. 2026b), particularly in the UV (Tang et al. 2025, Treiber et al. 2025), as well as Fe II emission, characteristic of the broad line region (BLR) of classical AGNs (e.g., Labbe et al. 2024, Tripodi et al. 2025a, Torralba et al. 2026a).

However, despite the high level of detail in this increasingly complex picture, the physical nature, origin, and evolution of these sources remain unclear. Several studies have attempted to fit LRD’s SEDs using well-known codes and different combinations of stellar and AGN models, trying to place these objects within the broader galaxy evolution framework (e.g., Greene et al. 2024, Pérez-González et al. 2024, Mérida et al. 2025, Tripodi et al. 2025b). Nevertheless, these attempts have failed to provide a unique prescription for LRDs, as the high stellar masses (M_*) or dust attenuations (A_V) invoked, especially in those cases with extreme Balmer breaks, conflict with our current understanding of stellar physics, mass surface densities, and the lack of X-ray and infrared (IR) emission of LRDs.

As a result, alternative solutions have been proposed, such as the black hole star (BH*) model (e.g., de Graaff et al. 2025c, Inayoshi & Maiolino 2025, Ji et al. 2025, Naidu et al. 2025, Rusakov et al. 2026), binary massive black holes (Inayoshi et al. 2025), the Super-Eddington Unification Model

* Corresponding author: Rosa.MeridaGonzalez@smu.ca

(Madau & Maiolino 2026), or direct collapse BHs (e.g., Baggen et al. 2026, Pacucci et al. 2026). Many of these theories share common physical ingredients and could ultimately be pieces of a broader and better-tailored framework for LRDs. However, they still require rigorous testing to determine whether they truly provide the solutions these sources demand.

One of the most popular theories in the current LRD paradigm is the BH* model. This idea envisions LRDs as accreting BHs whose emission is reddened by a dense envelope or cocoon of neutral gas ($n_H \sim 10^{9-11} \text{cm}^{-3}$, $N_H \sim 10^{24-26} \text{cm}^{-2}$), with a near-unity covering factor (Torralba et al. 2026b). Such a gas envelope would behave as a photosphere near the Hayashi limit, with temperatures $\sim 5000 - 7000 \text{K}$ (e.g., Inayoshi & Maiolino 2025, Kido et al. 2025, Inayoshi et al. 2026). From a theoretical perspective, the origin of such an envelope is expected to be linked to Super-Eddington accretion, whereas its disappearance could be driven by nuclear starbursts that expel the surrounding gas reservoir, effectively starving the envelope (Inayoshi et al. 2026). Observationally, the evolution of these sources may proceed in different ways (e.g., by growing a stellar outskirt, Billand et al. 2026; by losing the steep optical slope linked to the envelope, Asada et al. 2026, Mérida et al. 2026a), and a few LRDs might even survive to the present day in the local Universe.

Key evidence in favor of the BH* model was the discovery of “extreme” LRDs such as *The Cliff* (de Graaff et al. 2025c). This galaxy, located at $z_{\text{spec}} = 3.55$, exhibits a distinctive feature that ruled out a stellar origin, at least for some of these galaxies. *The Cliff* displays a break close to the Balmer limit that mimics a stellar break and has an extremely high strength of 6.9. de Graaff et al. (2025c) showed that a stellar origin for this source is highly improbable, as its compact size and high M_\star ($\sim 10^{10.5} M_\odot$) imply that it should emit significant X-ray radiation. In de Graaff et al. (2025b), the optical continuum of this source was fitted using a modified blackbody (BB) component, which depends on a scale parameter, temperature, and a power law whose slope modifies the BB. They found a median best-fit temperature for the modified BB emission of *The Cliff* of $T \sim 3974 \text{K}$, strongly supporting the picture that LRDs are AGN embedded in thermalized dense gas envelopes in approximate hydrostatic equilibrium.

However, the link between the rest-frame ultraviolet (UV) and optical emission of this now canonical LRD within the BH* model is not yet fully understood, nor is the origin of the LRD UV emission itself. The UV emission of LRDs is primarily attributed to a low-mass, star-forming, metal-poor, and dust-free galaxy host (e.g., Matthee et al. 2025, Pizzati et al. 2025, Lin et al. 2026b via clustering analysis; see also Korber et al. 2026, Sun et al. 2026, although see Barro et al. 2025 reporting $M_\star > 10^9 M_\odot$ and $A_V \sim 0.5 \text{mag}$ for some LRDs).

In many LRDs, the UV is spatially resolved, in line with the host hypothesis (e.g., Chen et al. 2025a, Rinaldi et al. 2025, Cloonan et al. 2026). However, such an interpretation would be in tension with the presence of high-ionization UV lines and Fe II emission in some LRDs. This suggests that a mixture of LRDs probably exists, with some being fully dominated by the host in the UV and others having some AGN contribution. The rest-frame UV emission of *The Cliff* is very compact, and there are no UV lines observed (de Graaff et al. 2025c). Thus, the UV emission could have either a stellar or an AGN origin.

So far, most observational LRD works that explore the constraints of the BH* model have focused either on a separate fit to the optical continuum emission, or on illustrative models that combine star-forming galaxy spectra and a BB emission (e.g.,

de Graaff et al. 2025c, Ji et al. 2025, Lin et al. 2025, Taylor et al. 2025, Sun et al. 2026, Umeda et al. 2026). These efforts have supported the BH* model and shed light on the possible sources of the two regimes of the “V”-shaped SEDs. However, it is crucial to test whether the entire spectrum of LRDs can be well reproduced at once by the BH* model and if the retrieved physical properties—derived from the full posterior distributions rather than from visual agreement—satisfy, on average, the LRD’s attributes.

A pioneering example of a UV-to-optical LRD spectral fitting was proposed in Barro et al. (2025), fitting a sample of 118 LRDs. They adopted a semiempirical model that combined a stellar and BH* components, with the BH* template being obtained by fitting a low-order polynomial to the emission line-free regions of *The Cliff* spectrum, assuming no BH* contribution to the UV. The BH* template is modified per galaxy through the A_V parameter only.

Barro et al. (2025) pointed out that the observed LRD diversity is primarily driven by variations in the BH*-to-galaxy luminosity ratio, together with increasing obscuration of the BH* component. For *The Cliff*, they obtained a best-fitting stellar mass of $\log M_\star/M_\odot = 8.67 \pm 0.63$ and stellar extinction of $A_V = 0.45 \pm 0.18 \text{mag}$, which is consistent with a low- or intermediate-mass system subject to moderate levels of dust attenuation; the A_V affecting the envelope is only $0.01 \pm 0.07 \text{mag}$. However, that study did not consider an AGN component and assumed a BB nature for the optical continuum, with a fixed temperature across all of their LRDs.

In this work, we use the spectral fitting code *Bagpipes* (Carnall et al. 2018), modified to include BB emission and a gas absorption component at the Balmer limit. Using PRISM data probing the rest-frame UV and optical continua, we conducted a comprehensive spectral analysis of *The Cliff*, examining the ability of the BH* model to describe this LRD and analyzing its host properties. Throughout this work, we assumed $\Omega_{M,0} = 0.3$, $\Omega_{\Lambda,0} = 0.7$, and $H_0 = 70 \text{km s}^{-1} \text{Mpc}^{-1}$. All M_\star and star formation rate (SFR) estimates assumed a Chabrier (2003) initial mass function (IMF).

2. Data and methodology

This work is based on *James Webb Space Telescope* observations of *The Cliff* obtained with the Near Infrared Spectrograph (NIRSpec; Jakobsen et al. 2022) in PRISM mode ($R \sim 100$) using the micro-shutter assembly. This galaxy corresponds to source #154183 from the Red Unknowns: Bright Infrared Extragalactic Survey (RUBIES; PIs: A. de Graaff & G. Brammer; de Graaff et al. 2025a). The data were obtained from version 4 of the DAWN JWST Archive (DJA; Brammer & Valentino 2025).

As mentioned in Sect. 1, current SED fitting codes, based only on stellar and AGN emission, cannot properly fit LRDs. One of the most promising explanations of the nature of LRDs is based on the presence of a dense gas envelope that is capable of obscuring the emission from the central engine, which is, however, a feature that most standard SED fitting codes do not explicitly model at present. de Graaff et al. (2025b) used a modified black body prescription to fit the optical continuum emission of a sample of LRDs (see also Barro et al. 2025). This gas cocoon has also been modeled in several works using *Cloudy* (Ferland et al. 2017; see Ji et al. 2025, Lin et al. 2025, Taylor et al. 2025 among many others).

In this work, we attempted to fit the full SED of *The Cliff* using a customized version of *Bagpipes*. This Python software utilizes a Bayesian inference approach and allows fitting

of the UV and optical emission from an AGN accretion disk using a double power-law model. The code also implements nonparametric star formation histories (SFHs) using a series of piecewise constant functions in lookback time. We used the continuity mode, based on the nonparametric SFH formulation of Leja et al. (2019), and all fits were performed using the Multinest sampling algorithm. A great advantage of *Bagpipes* is that it allows the user to include additional model components using the option `extra_components` in the `fit_dictionary`. The sum of all the components we use, described in Sec. 2.1, results in a total of 19 free parameters. Through these components and a set of priors, we can test different key elements of the BH* model.

2.1. Model components

In this subsection, we describe the priors chosen for each of the components introduced in the *Bagpipes* modeling. We adopted two main configurations: one called BH*+dust-free host and another called BH*+dusty host. These configurations are identical in all parameters except those that affect the stars, stellar metallicity, and dust of the stellar component. The BH*+dust-free host configuration aims to align with the expectation of the BH* model for the host of LRDs, indicating a metal-poor and dust-free, low-mass galaxy. The BH*+dusty host configuration explores a broader set of priors for the stellar component. If the former accurately represents nature, then both configurations should converge to the same low-mass, metal-poor, and dust-free solution.

We ran *Bagpipes* using these two configurations, each under two scenarios: (i) including the main optical-to-near IR emission lines, and (ii) masking them out. The emission lines were masked by assigning large uncertainties to both the lines and the surrounding continuum. This approach allows us to assess whether any discrepancies between the BH*+dust-free and dusty host configurations arise from constraints imposed by the continuum or by the emission lines. The redshift was set to $z_{\text{spec}} = 3.546$, as provided by the DJA and also specified in de Graaff et al. 2025c. All the priors are flat, and a summary of all the prior configurations is provided in Table 1.

– Blackbody emission

We can model the emission from a BB analytically using Planck’s law. In that way, we can introduce this component with just two parameters: temperature and a normalization factor, which accounts for the contribution of this component to the total solution. We set the allowed temperature range to $T = [1000, 7000]$ K and the normalization range to $\log A_{\text{BB}} = [-25, -16]$, with A_{BB} being expressed in units of $\text{erg/s/cm}^2/\text{\AA}$.

– Absorption

In *The Clifff*, the break located at the Balmer limit is very extreme (Balmer strength of 6.9), as a result of gas absorption. This is translated into a sharp drop in the optical continuum emission, which in our formulation should manifest as an equally sharp decline in the BB component at the Balmer limit. However, in the nominal Plank function the tail of this component does not fall off rapidly enough to reproduce such strong breaks. As a result, the BB tail extends into the UV unless it is suppressed explicitly.

To reproduce potential sharp spectral discontinuities observed around the Balmer limit, we introduced a phenomenological, data-driven absorption model analogous to the treatment

commonly adopted for the Lyman break:

$$\begin{aligned} F_{\text{final, BB}}(\lambda) &= B(\lambda) T(\lambda); \\ T(\lambda) &= e^{-\tau_B(\lambda)}; \\ \tau_B &= N \sigma_B(\lambda); \\ \sigma_B &= \sigma_{B_0} \left(\frac{\lambda}{\lambda_{\text{break}}} \right)^3 \sigma(\lambda); \\ \sigma(\lambda) &= \frac{1}{1 + e^{\left(\frac{\lambda - \lambda_{\text{break}}}{w} \right)}} \end{aligned} \quad (1)$$

In the above formulation, the intrinsic BB spectrum, $B(\lambda)$, is attenuated by a transmission function $T(\lambda)$, where τ_B represents an effective optical depth associated with the absorption of the Balmer continuum. We parametrized this optical depth as a function of N , an effective column density, and $\sigma_B(\lambda)$, a wavelength-dependent cross section. N is a column density, but it does not correspond directly to a physical N_H ; rather, it acts as a parameter that controls the strength of the break. Motivated by the bound-free absorption of hydrogen, the cross section is assumed to scale as $\sigma_B(\lambda) \propto (\lambda/\lambda_{\text{break}})^3$ below the Balmer edge. To avoid a nonphysical, overly sharp discontinuity, we introduced a smooth transition function modeled as a logistic function, $\sigma(\lambda)$, with characteristic width w , which regulates the onset of absorption across the break. In the fit, λ_{break} is allowed to vary around the vicinity of the Balmer limit. This absorption feature ($T(\lambda)$) and the BB spectrum are combined to produce the emission of the envelope, represented as a single curve in all our figures (i.e., $F_{\text{final, BB}}(\lambda)$).

In Appendix A, we present a fit to *The Clifff* without this absorption feature to demonstrate its effect. Without the gas absorption, the code attributes all the continuum emission to the BB, including the UV continuum. As a result, *Bagpipes* effectively eliminates the galaxy component in the fit. Without the absorption implemented in the model, LRDs such as *The Clifff* could be interpreted as envelope-dominated systems, with absent or negligible hosts. However, this setting does not yield a robust fit, as highlighted by the residuals and the reduced χ^2 values, emphasizing the need for the inclusion of the absorption component.

– Stars + Nebular emission + Dust attenuation

The stellar metallicity prior was set to span $\log Z/Z_{\odot} = [0.001, 0.05]$ in the BH*+dust-free host configuration, forcing a low- Z solution, and extended to $[0.001, 2.5]$ in the BH*+dusty host configuration. In terms of stellar mass, LRD hosts are expected to be low-mass sources (see Sect. 1), with $M_{\star} \sim 10^{7-8} M_{\odot}$. In the BH*+dust-free host configuration, $\log M_{\star}/M_{\odot}$ was set to span $[4.0, 8.5]$. In the BH*+dusty host mode, this prior was broadened to $[4.0, 10.0]$.

Nebular emission was incorporated through the ionization parameter, $\log U$, whose prior was set to span $[-4, 0]$. We selected a Small Magellanic Cloud (SMC) extinction curve (Gordon et al. 2003), which acts only on the nebular and stellar emission, with A_V values ranging over $[0, 0.5]$ mag and $[0, 5]$ mag in the BH*+dust-free and dusty host configurations, respectively. We explored selecting a Calzetti et al. (2000) dust attenuation law instead in Sect 4.1.

– AGN

The AGN continuum emission was modeled as a broken power law characterized by three parameters: two spectral slopes

Table 1: `Bagpipes` priors used in this work

SFH	Nebular	Dust	AGN	BB	Absorption
bin_edges = [0, 10, 30, 100, 300, 700, 900] massformed = [4, 8.5] and [4, 10] metallicity = [0.001, 0.05] and [0.001, 2.5]	log U = [-4, 0]	A_V = [0, 0.5] and [0, 5]	alphalam = [-2.8, 2] betalam = [0.8, 1.6] hanorm = [0, 5×10^{-16}] f5100A = [0, 3×10^{-16}]	T = [1000, 7000] log A = [-25, -16]	log sigma_B0 = [-18, -15] log N = [19, 24] λ_{break} = [3000, 4000] break_width = [10, 100]

Notes. `Massformed`, `metallicity`, and A_V show two different ranges, corresponding to the BH*+dust-free and dusty host configurations. The SFH is set to the continuity mode, and the bins are expressed in Myr. $dSFR_i$, which represents the change in log SFR between two consecutive SFH bins, is set to [-10, 10], following a Student-t distribution. The `massformed` parameter is logarithmic and in M_\odot units; the `metallicity` is logarithmic and in Z_\odot units; A_V is in magnitudes; `hanorm` has units of $\text{erg/s/cm}^2/\text{\AA}$ and `f5100A` is in $\text{erg/s/cm}^2/\text{\AA}$; λ_{break} and `break_width` are in units of \AA . The normalization factor of the BB, A, is expressed in $\text{erg/s/cm}^2/\text{\AA}$ and the temperature is in K. In the absorption component, the $\text{sigma_B0} \times N$ product is dimensionless. In total, we work with 19 free parameters.

$(\alpha_\lambda, \beta_\lambda)$ and the continuum flux at the break point (5100 \AA ; `f5100A`). The AGN line emission was included as H β and H α lines. The intensities were left free (`hanorm`), while the line widths were fixed through the H α line width as measured by us from the spectrum.

According to the BH* model, the dense gas envelope reprocesses the AGN emission, thereby eliminating any potential AGN contribution to the UV and optical continua. Although the origin and nature of the broad Balmer lines is still under debate (e.g., electron scattering through nuclear dense plasma, Rusakov et al. 2026; BLR stratification, Scholtz et al. 2026; hard, ionizing-rich intrinsic SEDs and an anisotropic radiation field, Madau & Maiolino 2026; young massive stars surrounding the envelope, Asada et al. 2026), in this work we assumed that they are originating in the BLR, as in Type I AGNs. We acknowledge that this is a caveat in our test to probe the BH* model and that additional mechanisms for the broad Balmer emission should be explored in future works.

However, the `Bagpipes` AGN model does not include hydrogen lines beyond H α and H β . As a result, any additional line emission is necessarily attributed to the host galaxy in the fit. Furthermore, `Bagpipes` uses Gaussian profiles for the broad line components and does not capture more complex line profiles, such as those observed in the Balmer lines of *The Cliff* (de Graaff et al. 2025c). Repeating the fits with the lines masked, considering only the flux from the continuum (see Sect. 3), ensures that the emission lines—potentially contaminated by the AGN—are not key drivers in our modeling.

The contribution of the AGN continuum was set through the normalization parameter `f5100A` whose prior spans [0, 3×10^{-16}] $\text{erg/s/cm}^2/\text{\AA}$, with `f5100A` being a key parameter in our modeling. A low AGN normalization favors a stellar origin for the UV continuum within the model. In this configuration, `Bagpipes` is free to explore both AGN-dominated and AGN-suppressed solutions. A key point here is that a preference for low `f5100A` values would therefore provide independent support for the BH* scenario as it would emerge from the data rather than being enforced by the adopted priors.

The slopes priors were set to span $\alpha_\lambda = [-2.8, 2]$ and $\beta_\lambda = [0.8, 1.6]$. These values enable the AGN to produce steep UV slopes (i.e., a quasar-like UV spectrum with an unobscured accretion disk) while maintaining a weak optical continuum. Such steep UV slopes are not allowed within the BH* framework; however, we want to test whether the code can fully reproduce the UV with stars, or else it needs to invoke an AGN model with a steep UV slope.

Any UV leakage from the AGN would challenge the current BH* model assumption of a fully suppressed AGN component,

although this possibility cannot be ruled out given the presence of high-ionization UV lines in some LRDs (see Sect. 1), suggesting that ionizing radiation may escape along certain lines of sight (e.g., due to a clumpy envelope or a non-spherical configuration). However, with this test and priors, we are implicitly assuming that if the gas envelope does not suppress AGN-powered lines, it will also fail to suppress part of the AGN UV continuum; an assumption that may not hold if these lines are emitted from less buried regions (see Torralba et al. 2026a). Nevertheless, testing a more complex configuration is beyond the scope of this work.

3. Results

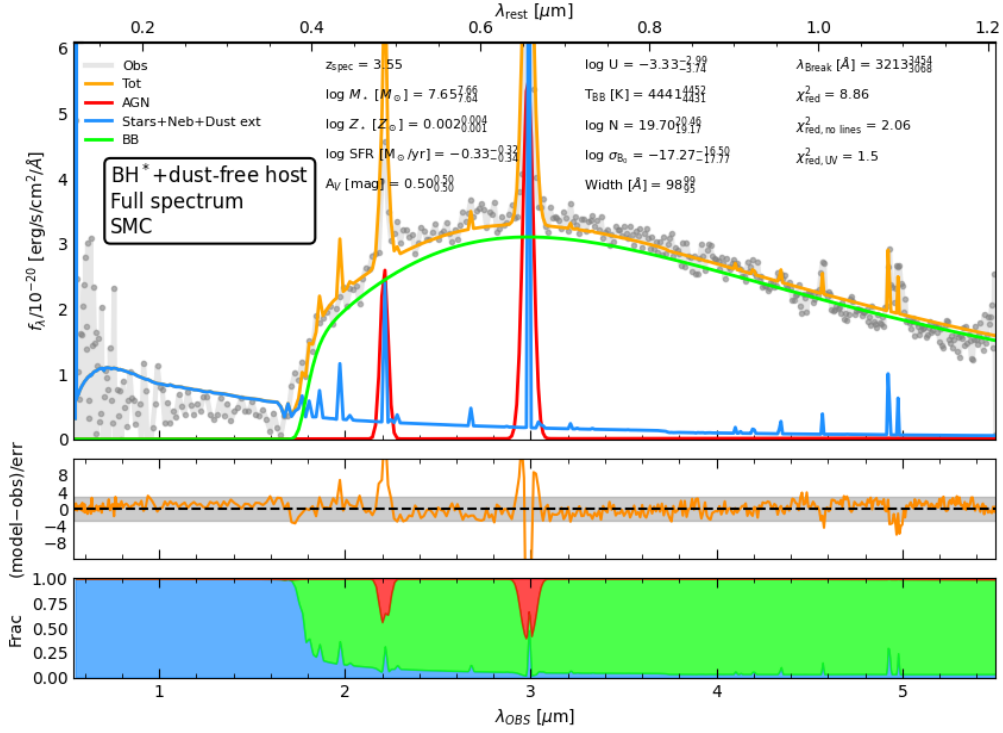
The `Bagpipes` best-fitting models for *The Cliff* according to both configurations, BH*+dust-free and dusty hosts, are depicted in Figs. 1 and 2, respectively. In each figure, we show the fits based only on the continuum and on the full spectrum, including the lines. A list of the values for all parameters can be found in Table 2.

A key result is that across all fits and configurations, and despite wide priors, `Bagpipes` consistently converges toward a low AGN normalization, effectively suppressing the AGN continuum and assigning most of the UV emission to stars and most of the optical emission to the BB component. This is exactly in line with the expectations of the BH* model. It is very compelling evidence for the validity of the BH* model, as this result is not based on any prior assumptions.

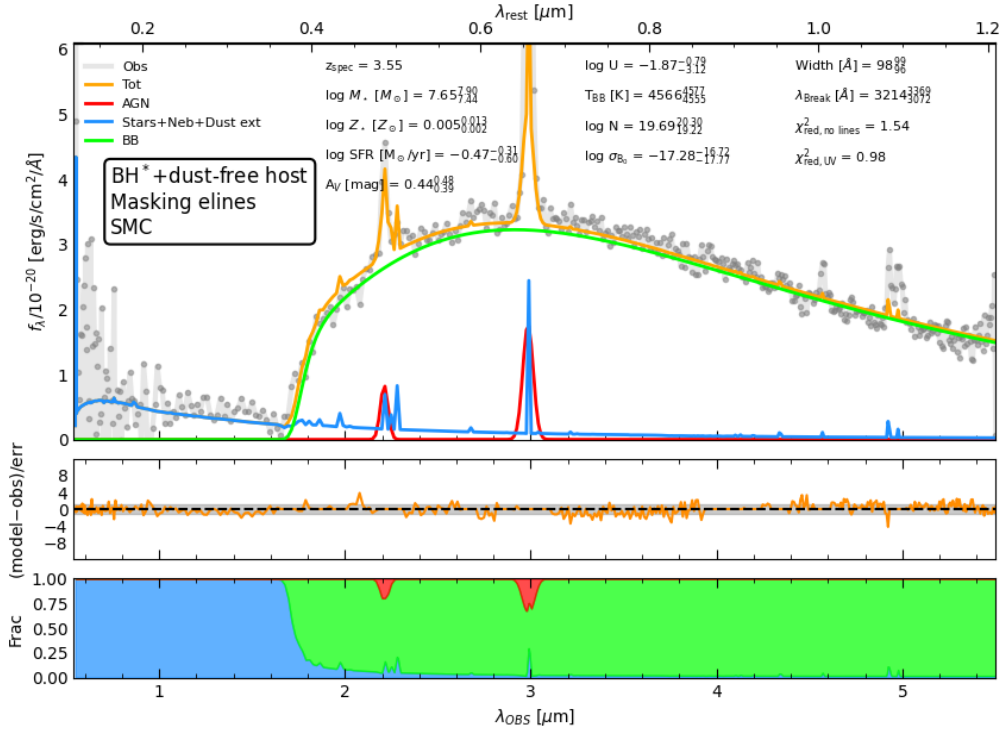
The fit also informs us about the properties of the host galaxy. Looking at Fig. 1, which shows the results for the BH*+dust-free host configuration, we find that *The Cliff* is described as a $\sim 10^{7.7} M_\odot$ galaxy with A_V close to the upper limit of the prior (0.5 mag). Some level of dust attenuation is therefore required by the fit, effectively ruling out an $A_V = 0$ mag scenario for this LRD.

The log SFR₁₀₀ values (which correspond to the SFR measured over the past 100 Myr) locate the host within the Main Sequence (MS) scatter of the Mérida et al. (2026b) MS relation at the low-mass end at this redshift. Meanwhile, the BB temperature varies between 4,441 and 4,566 K, depending on whether emission lines are included, while the parameters defining the gas absorption are similar in both cases.

The main difference between the two panels in Fig. 1 lies in the UV continuum fit. When fitting the full spectrum, including the emission lines (panel a), the model tends to overestimate the UV continuum, particularly at rest-frame $\lambda > 0.2 \mu\text{m}$, as reflected in the residuals and a reduced χ^2 value as measured in the UV ($\chi^2_{\text{red, UV}}$) of 1.5. In contrast, when masking the emission

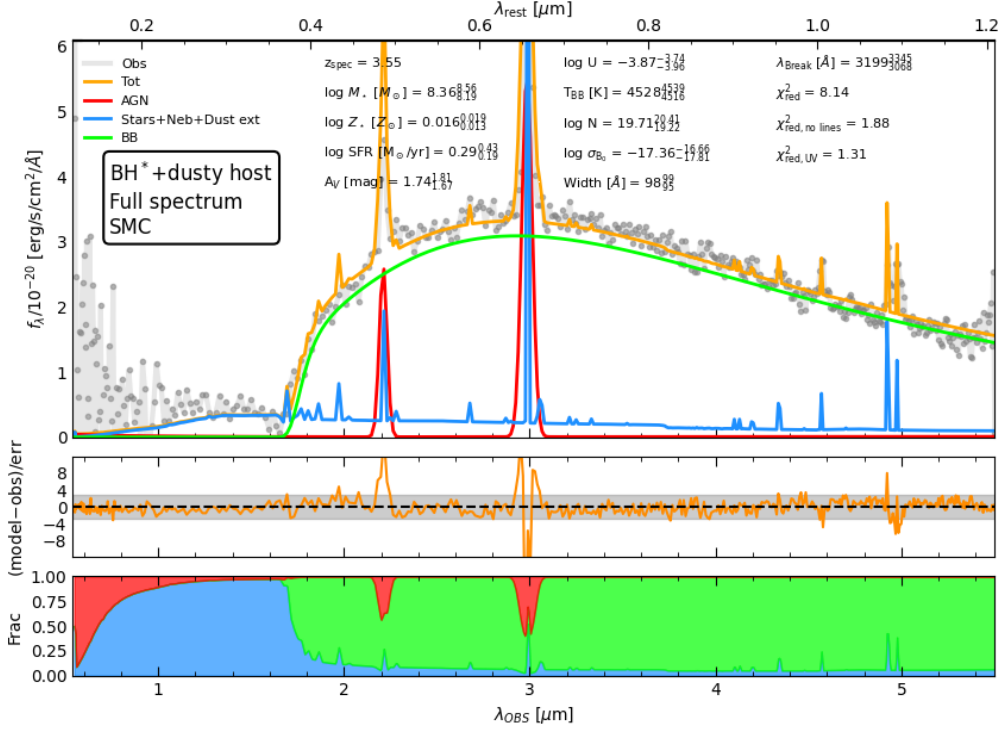


(a) SED fitting of *the Clifff* using the BH*+dust-free host configuration with an SMC law on the full spectrum.

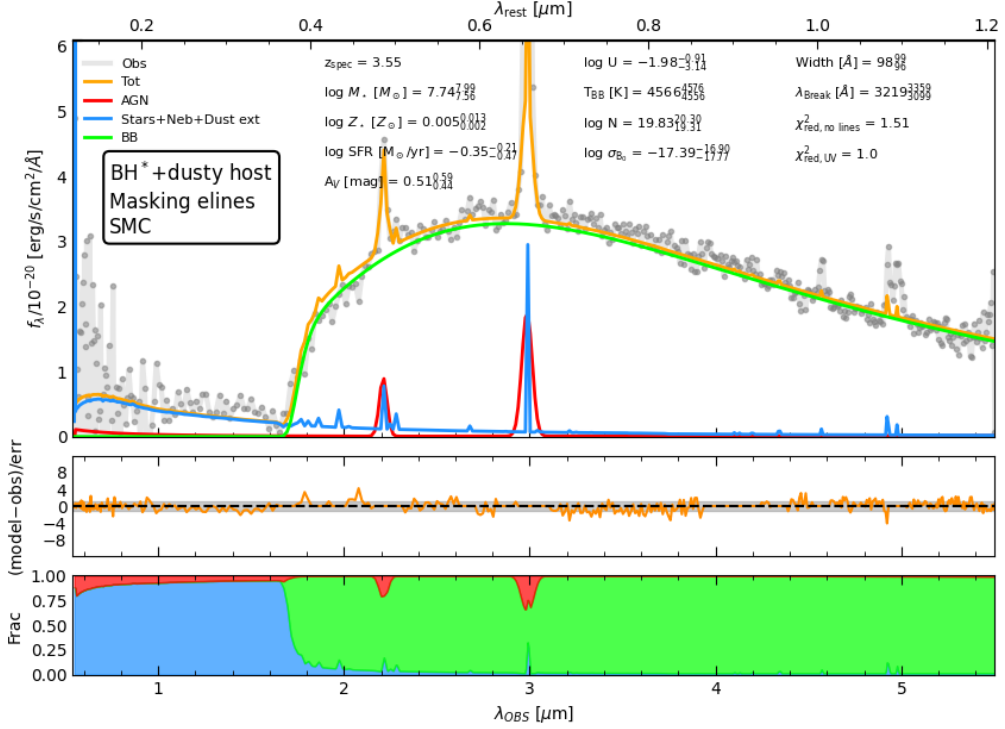


(b) SED fitting of *the Clifff* using the BH*+dust-free host configuration with an SMC law on the continuum.

Fig. 1: Best-fitting models from *Bagpipes* using the BH*+dust-free host configuration for *The Clifff*. The top panel shows the fit based on the full spectrum, whereas the second panel considers only the flux from the continuum. In both panels, the observed spectrum is shown in gray. We include the total best-fitting model (orange), the AGN component (red), the stellar + nebular component, attenuated by dust (blue), and the composite of the BB and Balmer absorption (green). The stellar + nebular model overlays with the total best-fitting model in the UV. We include three reduced χ^2 values: based on the full spectrum, based only on the continuum, and measured only in the UV. The residuals of the fit are depicted underneath each SED plot. The shaded gray region represents the standard deviation. The fractional contribution of each component to the total best-fitting model is displayed in the bottom rows, following the same color code as above. These fits indicate that *The Clifff* requires a moderate level of dust attenuation.



(a) SED fitting of *the Cliff* using the BH*+dusty host configuration with an SMC law on the full spectrum.



(b) SED fitting of *the Cliff* using the BH*+dusty host configuration with an SMC law on the continuum.

Fig. 2: Best-fitting models from Bagpipes using the BH*+dusty host configuration for *The Cliff*. The top panel shows the fit based on the full spectrum, whereas the second panel only considers the flux from the continuum. See Fig. 1 for a full description of the markers and color codes shown here. Results based on the continuum match those obtained with the BH*+dust-free configuration, but higher A_V and M_* values are retrieved when the full spectrum is considered.

lines and fitting only the continuum (panel b), the model slightly underestimates the UV flux but achieves a better overall match with the data, especially in the UV, with a $\chi^2_{\text{red, UV}} = 0.98$.

The BH*+dusty host configuration, shown in Fig. 2, matches the BH*+dust-free fit only if the emission lines are not taken into account. If the full spectrum is used, the code provides even

Table 2: Properties of *The Cliff* as measured in this work.

	BH* +dust-free host		BH* +dusty host			
	SMC		SMC		Calzetti	
	Full spectrum	Continuum	Full spectrum	Continuum	Full spectrum	Continuum
$\log M_*/M_\odot$	$7.65^{7.66}_{7.64}$	$7.65^{7.90}_{7.44}$	$8.36^{8.56}_{8.19}$	$7.74^{7.99}_{7.56}$	$8.26^{8.41}_{8.18}$	$8.12^{8.30}_{7.95}$
$\log Z/Z_\odot$	$0.002^{0.004}_{0.001}$	$0.005^{0.013}_{0.002}$	$0.016^{0.019}_{0.013}$	$0.005^{0.013}_{0.002}$	$0.015^{0.018}_{0.012}$	$0.013^{0.020}_{0.005}$
$\log U$	$-3.33^{2.99}_{-3.74}$	$-1.87^{0.79}_{-3.12}$	$-3.87^{3.74}_{-3.96}$	$-1.98^{0.91}_{-3.14}$	$-3.88^{3.76}_{-3.96}$	$-1.95^{0.96}_{-3.09}$
A_V [mag]	$0.50^{0.50}_{0.50}$	$0.44^{0.48}_{0.39}$	$1.74^{1.81}_{1.67}$	$0.51^{0.59}_{0.44}$	$1.78^{1.84}_{1.72}$	$1.04^{1.14}_{0.94}$
$\log \text{SFR}_{100}$ [M_\odot/yr]	$-0.33^{0.32}_{-0.34}$	$-0.47^{0.31}_{-0.60}$	$0.29^{0.43}_{0.19}$	$-0.35^{0.21}_{-0.47}$	$0.24^{0.35}_{0.20}$	$-0.04^{0.08}_{-0.17}$
α_λ	$0.18^{1.47}_{-1.37}$	$-0.38^{1.09}_{-1.76}$	$-2.74^{2.67}_{-2.78}$	$-2.37^{2.08}_{-2.63}$	$-0.70^{0.77}_{-2.08}$	$-0.93^{0.35}_{-2.00}$
β_λ	$1.14^{1.41}_{0.94}$	$1.13^{1.42}_{0.91}$	$0.85^{0.93}_{0.81}$	$1.08^{1.29}_{0.91}$	$1.15^{1.38}_{0.94}$	$1.15^{1.37}_{0.95}$
hanorm [erg/s/cm ²]	$3.98^{3.98}_{3.89} \times 10^{-17}$	$8.32^{13.49}_{3.39} \times 10^{-18}$	$3.89^{3.89}_{3.80} \times 10^{-17}$	$8.51^{13.80}_{4.47} \times 10^{-18}$	$3.89^{3.89}_{3.80} \times 10^{-17}$	$9.12^{14.13}_{4.47} \times 10^{-18}$
f5100 [erg/s/cm ² /Å]	$2.88^{7.24}_{0.78} \times 10^{-23}$	$5.01^{11.22}_{1.74} \times 10^{-23}$	$1.00^{1.20}_{0.81} \times 10^{-21}$	$7.41^{17.38}_{2.34} \times 10^{-23}$	$5.13^{10.96}_{1.55} \times 10^{-23}$	$5.89^{12.59}_{1.95} \times 10^{-23}$
T _{BB} [K]	4441^{4452}_{4431}	4566^{4577}_{4555}	4528^{4539}_{4516}	4566^{4576}_{4556}	4499^{4509}_{4489}	4573^{4582}_{4564}
A _{BB} [erg/s/cm ² /Å]	$1.41^{1.45}_{1.41} \times 10^{-19}$	$1.48^{1.48}_{1.48} \times 10^{-19}$	$1.41^{1.41}_{1.41} \times 10^{-19}$	$1.48^{1.48}_{1.48} \times 10^{-19}$	$1.41^{1.41}_{1.41} \times 10^{-19}$	$1.48^{1.48}_{1.48} \times 10^{-19}$
$\log N$	$19.70^{20.46}_{19.17}$	$19.69^{20.30}_{19.22}$	$19.71^{20.41}_{19.22}$	$19.83^{20.30}_{19.31}$	$19.72^{20.42}_{19.26}$	$19.62^{20.21}_{19.24}$
$\log \sigma_{B_0}$	$-17.27^{16.50}_{-17.77}$	$-17.28^{16.72}_{-17.77}$	$-17.36^{16.66}_{-17.81}$	$-17.39^{16.90}_{-17.77}$	$-17.33^{16.77}_{-17.71}$	$-17.34^{16.79}_{-17.74}$
Width [Å]	98^{99}_{95}	98^{99}_{96}	98^{99}_{95}	98^{99}_{96}	98^{99}_{95}	98^{99}_{96}
λ_{break} [Å]	3213^{3454}_{3077}	3214^{3369}_{3072}	3199^{3345}_{3068}	3219^{3359}_{3099}	3210^{3377}_{3078}	3213^{3405}_{3088}
χ^2_{red}	8.86		8.14		8.25	
$\chi^2_{\text{red, no lines}}$	2.06	1.54	1.88	1.51	1.84	1.46
$\chi^2_{\text{red, UV}}$	1.50	0.98	1.31	1.00	0.89	0.96

Notes. The values correspond to the median and 16th and 84th percentiles. We distinguish between the results obtained using an SMC (Sect. 3) and a Calzetti (Sect. 4.1) dust attenuation laws, and we further separate the solutions derived from continuum-only fits from those based on the full spectrum. SFR₁₀₀ corresponds to the SFR measured over the past 100 Myr. We include the reduced χ^2 values associated with the best-fitting models. $\chi^2_{\text{red, no lines}}$ values were computed considering only the emission from the continuum, and $\chi^2_{\text{red, UV}}$ refers specifically to the UV continuum.

more dust attenuation ($A_V \sim 1.8$ mag, well outside the limits of the BH*+dust-free host configuration prior), higher M_* ($\sim 10^{8.4} M_\odot$), and slightly higher metallicity ($\log Z/Z_\odot \sim 0.02$). We also obtain a higher SFR₁₀₀ value, close to the limit defined by the MS scatter.

The BB temperature ranges from 4,528 to 4,566 K, depending on the inclusion of the emission lines. The parameters defining the absorption are broadly consistent across configurations. The reduced χ^2 values are slightly better in this configuration than in the BH*+dust-free host case. However, the fit in the UV is comparatively worse when the full spectrum is fitted, being too suppressed at shorter wavelengths.

In summary, based on the analysis of the continuum, we found that *The Cliff* host is likely a low-mass ($10^{7.7} M_\odot$), star-forming galaxy, characterized by a low metallicity ($\log Z/Z_\odot = 0.005$), and a moderate level of dust $A_V \sim 0.5$ mag, with a gas envelope temperature of $\sim 4,566$ K. If emission lines are considered, the dust attenuation and the M_* increase ($A_V \sim 1.8$ mag and $M_* \sim 10^{8.4} M_\odot$), as well as the SFR₁₀₀.

3.1. Comparison with previous analyses of *The Cliff*

In their analysis of *The Cliff*, de Graaff et al. (2025b) fitted a modified blackbody component to the optical part of the PRISM spectrum (see Sect. 1) and found a median blackbody temperature, along with the associated 16th and 84th percentiles, of $3,974^{4,033}_{3,919}$ K. The temperatures obtained using both their method and ours are consistent with those expected for a photosphere

near the Hayashi limit (Kido et al. 2025). As for the other physical parameters derived for *The Cliff* in this work, de Graaff et al. (2025b) did not explore stellar or AGN properties in an SED-fitting context.

Barro et al. (2025) reported best-fitting values for the M_* and attenuation of *The Cliff* using the SMC dust law. They found $\log(M_*/M_\odot) = 8.67 \pm 0.63$ and $A_V = 0.45 \pm 0.18$ mag. Their A_V estimate is consistent with our results, but their M_* is higher than our values, even within uncertainties. A comparable M_* is only recovered by our fits when adopting the BH*+dusty host configuration and fitting the full spectrum, without masking the lines. However, this solution requires a much higher attenuation, $A_V \sim 1.7$ mag, than that found by Barro et al. (2025). In addition, under these premises, Bagpipes assigns all emission line features, except the broad H α and H β components, to stellar processes. This effectively maximizes the contribution of the stellar component to the fit. Consequently, this scenario should be regarded as an upper limit on the M_* , suggesting that the true M_* is likely below $10^{8.4} M_\odot$.

4. Discussion

4.1. The dusty nature of the host of *The Cliff*

As a result of our fits, we reject a pure dust-free scenario for this LRD. The required level of dust attenuation depends heavily on the emission lines, but it is never $A_V \sim 0$ mag. Without any line emission constraints, the code requires $A_V \sim 0.5$ mag. This could

imply varying levels of dust acting on the stellar and nebular components depending on the stellar contribution to the lines. The maximum value would be an $A_V \sim 1.8$ mag, corresponding to the maximum possible contribution of the host to the emission lines.

These results are based on assuming an SMC extinction law, commonly used in LRD studies (e.g., Akins et al. 2025b, Barro et al. 2025, Ji et al. 2025, Taylor et al. 2025, Jones et al. 2026). In this subsection, we explore the effect of this assumption on the dust budget of *The Cliff*. For this goal, we repeated our analysis choosing a Calzetti et al. (2000) dust attenuation law, also used in a variety of LRD studies (e.g., Chen et al. 2025a, de Graaff et al. 2025c, Kocevski et al. 2025, Rinaldi et al. 2025, Umeda et al. 2026). Tripodi et al. (2025b) found this law to be consistent with an LRD at $z \sim 8.6$ using a flexible analytical attenuation model that was broadly compatible with a Calzetti-like curve, although slightly shallower in the rest-frame UV.

We present the results for the BH*+dusty host using a Calzetti law in Fig. 3. A summary of the derived properties can be consulted in Table 2. When the full spectrum is considered, the results of the fit are consistent with those reported using an SMC law: a star-forming, $10^{8.3} M_\odot$ host with $A_V \sim 1.8$ mag. However, the fit in the UV improves when we consider a Calzetti law, as this law is less steep in the UV and consequently suppresses the stellar component to a lesser extent.

If emission lines are masked, M_\star drops ($\sim 10^{8.1} M_\odot$), but this value is still higher than the results obtained for the SMC law based on the continuum alone. Metallicity is low, but higher than in the SMC case ($\log Z/Z_\odot = 0.013$). Moreover, the required A_V decreases only down to ~ 1 mag, significantly beyond the limits of the BH*+dust-free host A_V prior. The rest of the parameters are consistent with those obtained using an SMC law, including the BB temperature and the reduced χ^2 values.

This has important implications for the nature of LRD host galaxies. Depending on the assumed attenuation law and the stellar contribution to the emission lines, we infer significant dust attenuation in these systems, ranging 0.5 – 1.8 mag in the case of *The Cliff*. For context, normal star-forming galaxies of similar M_\star show $A_V \sim 0.3$ mag at these z (Merida et al. 2023). However, we cannot discriminate between a moderately or highly dust-obscured host through the data, as these A_V values remain consistent with the upper limits found for the LRDs’ dust mass from Atacama Large Millimeter/submillimeter Array (ALMA) 1.3 mm continuum observations ($\sim 10^6 M_\odot$, Casey et al. 2025), assuming effective radii of ~ 100 pc (Baggen et al. 2023, Guia et al. 2024) and the $M_d - A_V$ calibration from Ferrara (2024).

Differences in the A_V upper limits depending on the selected attenuation law were also reported in Chen et al. (2025b). That work used the SMC, Milky Way, and Orion Nebula attenuation laws to estimate the upper limits on A_V of LRDs from their predicted IR fluxes using data from the JWST Mid-Infrared Instrument, *Herschel*, and ALMA. They found that extinction curves that are steeper in the UV (like SMC) result in stronger UV attenuation for a given A_V , leading to larger reprocessed IR fluxes, and thus a stricter A_V upper limit, in line with our results. These authors derived upper limits of $A_V \leq 1 - 1.5$ mag for the brightest LRDs to date, A2744-45924 (Labbe et al. 2024) and RUBIES-BLAGN-1 (Wang et al. 2025), and for stacked SEDs from a large sample of LRDs, further supporting a dusty nature for the hosts of these objects.

4.2. The role of the AGN continuum in the UV

Our setup allows for the possibility of leakage of the AGN continuum into the UV, even for low values of the f5100A parameter, which sets the normalization of the AGN component. This regime corresponds to negative values of the slope α_λ , which governs the UV shape of the AGN continuum.

We found negative α_λ values in all configurations (see also the α_λ values derived using a Calzetti dust attenuation law), except for the BH*+dust-free host setup based on the continuum (see Table 2). However, α_λ plays a negligible role in the BH*+dust-free host configuration, as the f5100A parameter is sufficiently low to effectively suppress the AGN continuum. This is reflected by the fractional contribution of each component to the total model shown in each panel in Fig. 1.

In contrast, a small AGN contribution is present when using the BH*+dusty-host configuration (see Fig. 2). However, this contribution remains very low: the AGN UV component accounts for only 2 – 4% of the total best-fitting model, with the lower value obtained when fitting the full spectrum. The inferred AGN fractions—8% of the UV model flux when using the continuum and 19% when fitting the full spectrum—are comparable to the intrinsic degeneracies of the Bagpipes fitting. Nevertheless, they may also be hinting at a genuine physical contribution from the AGN, such that the UV continuum is a combination of AGN and host galaxy emission. So far, no UV emission lines have been detected in *The Cliff*, but the available medium-resolution spectroscopic data do not extend blueward of H α , preventing any direct assessment of the UV line spectrum.

In practice, AGN leakage in the model arises from the interplay between the stellar, nebular, and AGN components through dust attenuation, which does not affect the AGN model by construction. To some extent, the code attempts to suppress the stellar contribution to the UV continuum (powered by young stellar populations that produce a hard ionizing radiation field) using dust attenuation. This effectively weakens the coupling between the UV continuum and the nebular line production. At the same time, a modest AGN contribution helps reproduce the observed UV continuum without increasing the ionizing photon budget.

The preference of the model for a dustier solution with modest AGN UV leakage cannot be dismissed outright, as the resulting reduced χ^2 values remain consistent with statistically acceptable fits. In other words, if such leakage were physically present, the model would still be capable of capturing it while producing a BH*-like solution.

At the same time, this leaves open the possibility that the UV continuum could be entirely AGN-driven, with negligible contribution from the host. To test this scenario, we reran the code after removing the stellar, nebular, and dust attenuation components from the fit. The corresponding results, based on the continuum, are presented in Appendix B. The overall reduced χ^2 value is worse here, especially in the UV. The AGN is mostly suppressed through the normalization in the optical, but the UV slope makes it possible for the AGN to produce most of the UV emission. However, the best-fitting model underestimates the flux at $\lambda > 0.2 \mu\text{m}$, potentially ruling out a host-less scenario in this LRD.

In Appendix B, we also divided the α_λ prior into two distinct regimes, an unobscured AGN ($\alpha_\lambda = [-2.8, -1.8]$) and an obscured AGN regimes ($\alpha_\lambda = [0, 1]$). This experiment effectively forces the model to explore both a quasar-like UV continuum (i.e., allowing for AGN UV leakage) and a reddened AGN solution (i.e., suppressing AGN UV leakage by construction). We found that both regimes yield statistically indistinguishable

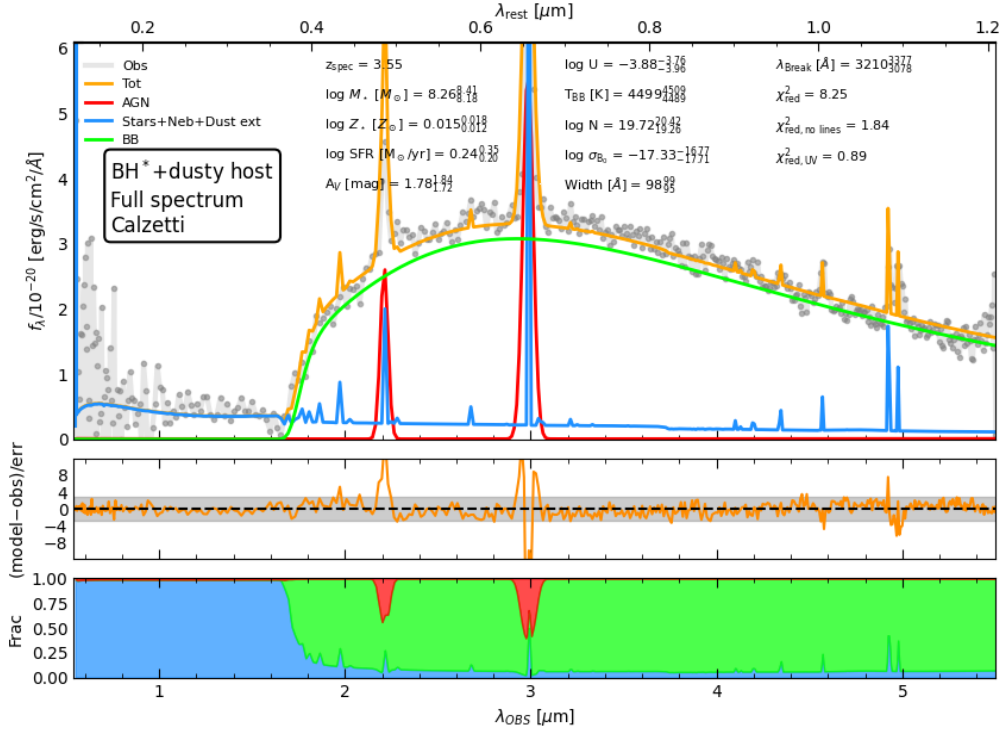
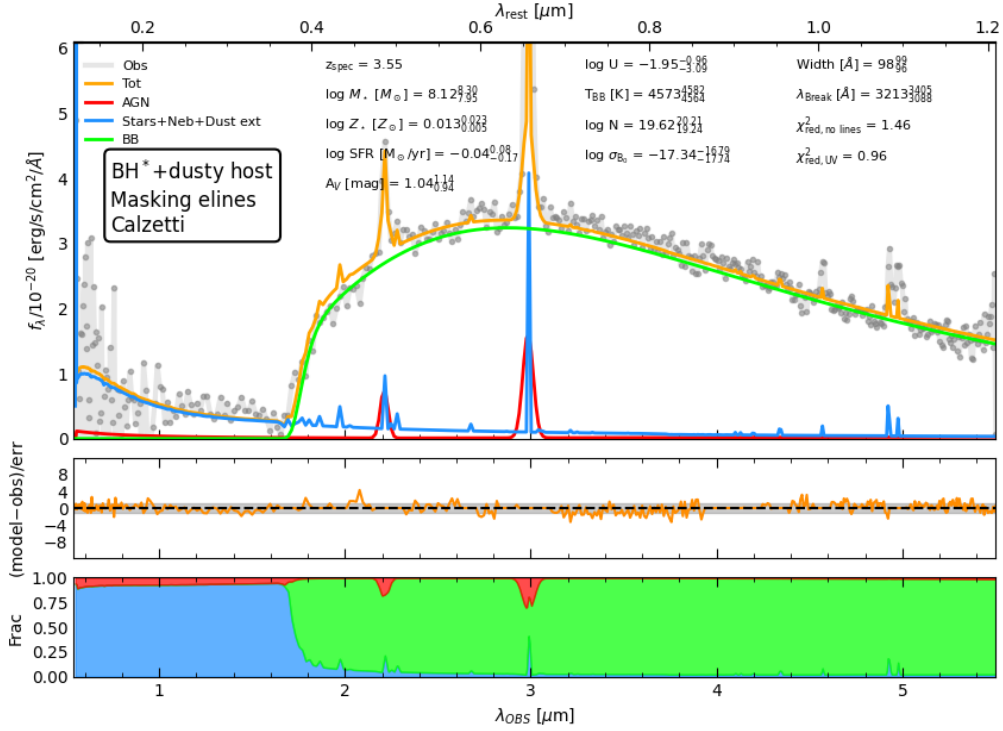

 (a) SED fitting of *the Cliff* using the BH*+dusty host configuration with a Calzetti law on the full spectrum.

 (b) SED fitting of *the Cliff* using the BH*+dusty host configuration with a Calzetti law on the continuum.

Fig. 3: Best-fitting models from *Bagpipes* using the BH*+dusty host configurations for *The Cliff* and a Calzetti et al. (2000) dust attenuation law. The top panel shows the fit based on the full spectrum, whereas the second panel only considers the flux from the continuum. See Fig. 1 for a full description of the markers and color codes shown here. The use of a Calzetti law yields higher A_V and M_* values when the continuum is considered.

fits. In other words, a purely stellar-driven UV continuum and a mixed AGN+stellar UV continuum remain degenerate solutions.

It is worth noting that a UV continuum that is not solely host-driven, together with weak [OIII] emission, such as that observed in *The Cliff*, is a scenario that can be naturally ex-

plained within the unified AGN framework for LRDs proposed by Madau & Maiolino (2026). According to this theory, LRDs host a super-Eddington central engine and differ primarily from compact Type I AGN by orientation and line-of-sight obscuration. The central engine is modeled as a geometrically thick radiation-pressure-supported accretion flow whose funnel produces strongly anisotropic, intrinsically blue ionizing continua. This is coupled to an equatorially concentrated broad-line region and a dusty reprocessing screen with a modest covering factor. Madau & Maiolino (2026) pointed out that weak [OIII] emission in LRDs with the strongest Balmer breaks may not require a host-dominated UV continuum, as is the case for luminous quasars. The [OIII] equivalent width in these systems is known to decrease with increasing luminosity (Baldwin 1977). This would imply high intrinsic luminosities in [OIII] weak, Balmer break LRDs, which could be the case for *The Cliff*, as strong Balmer breaks correspond to the most dust-attenuated sightlines. The compact Type I AGN counterparts of these sightlines potentially overlap with the quasar regime.

4.3. The Star Formation and Black Hole Growth History of *The Cliff*

In this subsection, we attempt to examine the SFH of *The Cliff*'s host and relate it to the BH accretion history. For this exercise, we cannot rely on the most recent SFH, as it is inferred from the emission lines powered by star formation. At present, we cannot disentangle the AGN contribution from the nebular emission of the host, making the SFH at < 10 Myr highly uncertain due to the likely contamination of the key SFR-tracing emission lines by the AGN. Moreover, the interplay between dust attenuation, stars, and nebular emission can also bias the SFR estimates on longer timescales (~ 100 Myr), which are probed by the UV continuum. These limitations imply that the results presented here should be interpreted with caution and regarded as exploratory.

Despite these caveats, there is observational evidence suggesting that at least part of the nebular emission may still safely trace recent star formation. Asada et al. (2026) found a tight correlation between the narrow-line component and the UV-to- $H\alpha$ luminosity ratio of a sample of $z > 5$ LRDs, consistent with that expected for young starburst galaxies. This trend was also observed for the broad $H\alpha$ component, albeit with a larger scatter. This implies that, in principle, the narrow $H\alpha$ component of *The Cliff* can be used to estimate its most recent star formation. Such an interpretation is further supported by the physics of the BH* model, as the gas envelope would prevent any AGN-driven narrow line emission from contaminating the spectrum.

The complex $H\alpha$ line profile of the *The Cliff* was explored in de Graaff et al. (2025c) using `unite` (Hviding et al. 2025) and the G395M spectrum. Their fiducial model assumed a broad Lorentzian and narrow Gaussian emission component, a narrow Gaussian absorption component, and a linear continuum. Assuming that the narrow component is only powered by stars, we can use the Kennicutt (1998) calibration for a Chabrier (2003) IMF and estimate the SFR from $H\alpha$. Considering a flux of 1.3×10^{-17} erg/s/cm² (de Graaff et al. 2025c), we estimate an $\text{SFR}(H\alpha) = 7 - 26 M_{\odot}/\text{yr}$, where the lower value corresponds to $A_V = 0$ mag and the upper value to $A_V \sim 1.8$ mag.

However, the full width at half maximum of the narrow $H\alpha$ component reported in de Graaff et al. (2025c) is 478 ± 95 km/s. This width is typical of AGN narrow lines, much higher compared to the typical values of 100 – 200 km/s of their stellar counterparts. This strongly suggests that the narrow $H\alpha$ emission in *The Cliff* is not purely stellar, and therefore cannot be

reliably used to trace star formation. As a result, the most recent SFH of LRDs remains unconstrained under the current limitations. A deeper understanding of the origin of LRDs' emission lines—and an assessment of whether such features can be produced within the BH* framework—is essential before robust SFR estimates can be derived.

With caveats about the reliability of SFR estimates in mind, especially at lookback times < 10 Myr, we proceed to examine *The Cliff*'s SFH. Figure 4 shows the SFH for *The Cliff* based on the BH*+dusty host setting, derived using the full spectrum and only the continuum. These tracks show $\text{SFR} \sim 0.01 - 1 M_{\odot}/\text{yr}$ at lookback times $\gtrsim 10$ Myr. If the full spectrum is considered, SFR increases to $\sim 10 M_{\odot}/\text{yr}$ at more recent lookback times.

This figure also includes the mass assembly history of *The Cliff*, derived by integrating the SFH while assuming a return fraction of 0.3 (i.e., as expected for a Chabrier 2003 IMF). We do this for the BH*+dusty host configuration based on the continuum. Note that, given its relative youth, assuming a constant return fraction of 0.3 likely overestimates the amount of recycled gas in this system. Thus, the $M_{\star}(t)$ could be somewhat higher, by up to ~ 0.3 dex, if we assumed lower return fractions. According to our results, the host galaxy increased its M_{\star} by only ~ 0.4 dex in the period ranging $\sim 10 - 300$ Myr in lookback time.

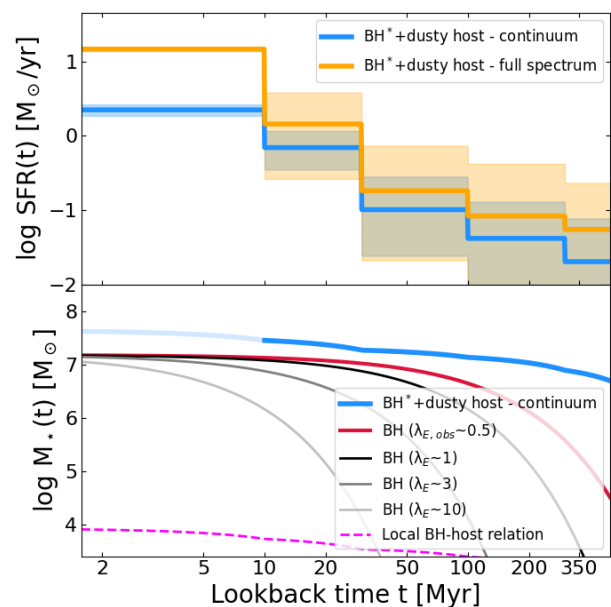


Fig. 4: Top: Star formation histories derived using the BH*+dusty host configuration based on the full spectrum (orange) and the continuum (blue). Shaded regions denote the area between the 16th and 84th percentiles, with the median represented as a solid line. Bottom: mass assembly history of *The Cliff* according to the BH*+dusty host configuration based on the continuum (blue). The curve is colored lighter at $t < 10$ Myr as a reminder of the lack of proper emission line constraints. Hypothetical growth tracks of the BH are included, assuming a final $M_{\text{BH}} = 10^{7.18} M_{\odot}$ and different Eddington accretion ratios. $\lambda_E \sim 0.5$ (red line) corresponds to the observed value. We depict three additional cases of Eddington (black) and super Eddington accretion (gray and silver). The evolution of a BH along the BH–host local relation from Reines & Volonteri (2015) is also displayed (fuchsia dashed line).

The theoretical predictions of Inayoshi et al. (2026) describe the assembling of the LRD hosts through an $\text{SFR} \geq 1 M_{\odot}\text{yr}^{-1}$

starburst, which led to the formation of a $\sim 10^7 M_\odot$ compact (≤ 100 pc) stellar cluster within ~ 10 Myr. In contrast, our results point to a much smoother evolutionary path: the galaxy appears to have been building up its M_\star over a longer period, with a $10^7 M_\odot$ host already in place ~ 200 Myr.

Even though we don't have information about the co-evolution of *The Cliff*'s host and the central engine, we can study the BH mass assembly history under certain assumptions. We can consider mass growth via accretion onto less massive seeds (Madau et al. 2014) and continuous gas supply along with uncorrelated accretion events. This ensures a soft duty cycle of $\sim 100\%$, which is a fair assumption for a gas-rich galaxy at these early epochs (Zubovas & King 2021). Following Madau et al. (2014) and if BH accretion is proportional to the BH mass, $\dot{M}_{BH} \propto M_{BH}$, as given by the $M - L$ relation, we can derive the time-dependent mass of the central BH as

$$\frac{dM_{BH}}{dt} = \frac{(1 - \epsilon) L}{\epsilon c^2} \text{ with} \quad (2)$$

$$M_{BH}(t) = M_{BH,0} \exp\left(\frac{(1 - \epsilon) \lambda_E}{\epsilon t_E} (t - t_0)\right),$$

where $M_{BH,0}$ is the mass of the BH seed, ϵ is the accretion efficiency, λ_E is the Eddington accretion ratio, and t_E is the Eddington timescale, defined as $t_E = M_{BH} c^2 / L_E = 0.44 \mu_e^{-1}$ Gyr (Madau et al. 2014). μ_e is the mean molecular weight per electron, which is 1.15 for primordial gas. Assuming this μ_e value and setting $\epsilon = 0.1$, we computed $M_{BH}(t)$ backward in time, starting with the current estimated M_{BH} .

The estimated M_{BH} for this object (without including a dust correction) is $\log(M_{BH}/M_\odot) = 7.18_{-0.06}^{+0.07}$ (de Graaff et al. 2025c), thus $M_{BH}/M_\star = 0.26$ (assuming a $M_\star = 10^{7.7} M_\odot$), well above the $M_{BH} - M_\star$ local relation (Reines & Volonteri 2015), as usually found for LRDs. This implies that *The Cliff* is a BH-dominated system. Its bolometric luminosity, assuming the scaling relations between $L_{H\alpha}$, L_{5100} , and L_{bol} of Greene & Ho (2005) and Shen et al. (2020), is $\sim 1 \times 10^{45}$ erg s $^{-1}$ (de Graaff et al. 2025c), which translates into a BH accretion rate of $0.18 M_\odot/\text{yr}$. The Eddington accretion ratio λ_E of *The Cliff*, defined as the ratio between the bolometric and Eddington luminosities, is ~ 0.5 . This object is thus accreting in a sub-Eddington regime. However, note that this approach assumes that the AGN is the primary driver of the $H\alpha$ emission, whereas the origin of the LRDs' broad Balmer lines is still a matter of debate. Additionally, M_{BH} should not exceed a few $10^7 M_\odot$ according to some BH* theoretical works (see $M_{crit,LRD}$ in Inayoshi et al. 2026), which is the mass at which the BH feeding rate is supposed to fall below the Eddington limit, preceding the end of the LRD phase. However, most reported LRD M_{BH} values are larger than this value (see Juodžbalis et al. 2025 and references therein), and the measured λ_E is already sub-Eddington in *The Cliff*. This points to a potential issue in the BH* model or a lack of accurate estimates of the BH properties in LRDs.

We estimated the mass assembly history of the BH for a constant $\lambda_E = 0.5$ and three additional cases, corresponding to Eddington and Super-Eddington accretion (see Fig. 4). All these growth tracks yield a BH growth that is incompatible with the local BH–host scaling relation, which predicts a final M_{BH} for *The Cliff* of $\sim 10^4 M_\odot$ based on the host's stellar mass. This tension could be partially alleviated if the BH experienced short episodes of super-Eddington accretion (e.g., Li et al. 2023, Lupi et al. 2024, Trinca et al. 2024, Quadri et al. 2025). However, even allowing for such bursts, the final M_{BH} cannot be reconciled with

a scenario in which the BH and its host coevolve along the local relation.

An alternative interpretation is provided by the direct collapse BH scenario (e.g., Pacucci et al. 2026; Baggen et al. 2026). In this framework, the tension in the host–BH coevolution naturally disappears, as the BH forms and grows independently of the stellar component. Subsequent interactions, such as migration of the BH into a low-mass companion galaxy, whose UV radiation suppressed molecular hydrogen cooling, thereby allowing the formation of these direct collapse BHs, could then explain the large M_{BH}/M_\star ratio estimated in *The Cliff*.

5. Conclusions

In this work, we tested the assumptions of the BH* model by performing a full UV-to-optical spectral fitting of *The Cliff* (de Graaff et al. 2025c) using JWST/NIRSpec PRISM data and a modified version of Bagpipes that includes blackbody emission and gas absorption at the Balmer limit. Our modeling naturally generates the BH* picture in this LRD without requiring strong constraints, indicating that this solution is driven by the data rather than imposed by the priors, and thereby providing a robust test of the BH* scenario.

Furthermore, according to our results there is a low-mass galaxy host in *The Cliff*, rendering the host-less scenario unlikely for this and similar LRDs. Our method thus provides a useful avenue for characterizing the hosts of LRDs even when they cannot be spatially resolved in imaging. The stellar component required by the fits constitutes potential evidence for the presence of a host galaxy in LRDs.

According to our fits to the spectral continuum, *The Cliff*'s host is a $\sim 10^{7.7} M_\odot$ metal-poor galaxy that evolves along the star-forming Main Sequence, in line with the expectations for LRD hosts within the BH* framework. However, this host is not dust-free, as it is subject to a mild dust attenuation ($A_V \sim 0.5$ mag under the SMC dust law), acting on the stellar and nebular components. Moreover, adopting a Calzetti et al. (2000) attenuation law instead of a Small Magellanic Cloud law yields larger M_\star and A_V values ($\sim 10^8 M_\odot$ and $A_V \sim 1$ mag), pointing toward an even more heavily obscured host.

In terms of the envelope, which dominates the optical continuum, we infer a blackbody temperature of ~ 4570 K. This value is fully consistent with theoretical expectations within the BH* framework, where the envelope behaves as a photosphere near the Hayashi limit.

In the BH* scenario, the AGN emission is reddened by this envelope, thus not contributing to the continuum. However, AGN continuum leakage in the UV is allowed and sometimes preferred by the code, which still preserves the overall BH* picture, even with a small contribution of the AGN to the UV continuum. A quasar-like UV continuum AGN (i.e., stellar+AGN-powered UV) is statistically indistinguishable from that of an obscured AGN (i.e., stellar-driven UV). A better understanding of the gas envelope's clumpiness, as well as the origin of potential high-ionization UV lines, will be key to shedding light on the AGN contribution to the UV emission of LRDs.

Finally, our fits also provide tentative insight into the evolutionary history of *The Cliff*. Its star formation history indicates a smooth evolutionary path, with a M_\star of $10^7 M_\odot$ already in place 200 Myr ago. The BH–host evolution consistently lies above the expectations from typical BH–host scaling relations, especially at recent times. Theories invoking direct collapse black holes (Pacucci et al. 2026) or the unified AGN framework (Madau & Maiolino 2026) offer potential explanations for the

potential lack of BH–host coevolution and the nature of the UV emission in LRDs which are not host-related. However, further testing with larger statistical samples of LRDs and higher resolution spectra is required to robustly test these models, as well as the BH* scenario.

Acknowledgements. We thank Jenny E. Green, David Setton, and Yilun Ma for valuable discussions and feedback that improved this work.

This research was enabled by Canadian Space Agency grants 18JWST-GTO1 and 24JWGO3A12 and Natural Sciences and Engineering Research Council (NSERC) of Canada grants RGPIN-2020-06023 and RGPAS-2020-00065.

The data products presented herein were retrieved from the Dawn JWST Archive (DJA). DJA is an initiative of the Cosmic Dawn Center (DAWN), which is funded by the Danish National Research Foundation under grant DNR140.

This research used the Canadian Advanced Network For Astronomy Research (CANFAR) platform operated in partnership by the Canadian Astronomy Data Centre and The Digital Research Alliance of Canada with support from the National Research Council of Canada, the Canadian Space Agency, CANARIE, and the Canada Foundation for Innovation.

This work is based on observations made with the NASA/ESA/CSA James Webb Space Telescope. The data were obtained from the Mikulski Archive for Space Telescopes at the Space Telescope Science Institute, which is operated by the Association of Universities for Research in Astronomy, Inc., under NASA contract NAS 5-03127 for JWST.

References

- Akins, H. B., Casey, C. M., Berg, D. A., et al. 2025a, *ApJ*, 980, L29
- Akins, H. B., Casey, C. M., Berg, D. A., et al. 2025b, *ApJ*, 980, L29
- Ananna, T. T., Bogdán, Á., Kovács, O. E., Natarajan, P., & Hickox, R. C. 2024, *ApJ*, 969, L18
- Asada, Y., Inayoshi, K., Fei, Q., Fujimoto, S., & Willott, C. 2026, arXiv e-prints, arXiv:2601.10573
- Baggen, J. F. W., Scoggins, M. T., van Dokkum, P., et al. 2026, arXiv e-prints, arXiv:2602.02702
- Baggen, J. F. W., van Dokkum, P., Labbé, I., et al. 2023, *ApJ*, 955, L12
- Baldwin, J. A. 1977, *ApJ*, 214, 679
- Barro, G., Perez-Gonzalez, P. G., Kocevski, D., et al. 2025, arXiv e-prints, arXiv:2512.15853
- Barro, G., Pérez-González, P. G., Kocevski, D. D., et al. 2024, *ApJ*, 963, 128
- Billand, J.-B., Elbaz, D., Gentile, F., et al. 2026, *A&A*, 706, A29
- Brammer, G. & Valentino, F. 2025, *The DAWN JWST Archive: Compilation of Public NIRSpect Spectra*
- Calzetti, D., Armus, L., Bohlin, R. C., et al. 2000, *ApJ*, 533, 682
- Carnall, A. C., McLure, R. J., Dunlop, J. S., & Davé, R. 2018, *MNRAS*, 480, 4379
- Casey, C. M., Akins, H. B., Finkelstein, S. L., et al. 2025, *ApJ*, 990, L61
- Casey, C. M., Akins, H. B., Kokorev, V., et al. 2024, *ApJ*, 975, L4
- Chabrier, G. 2003, *PASP*, 115, 763
- Chen, C.-H., Ho, L. C., Li, R., & Zhuang, M.-Y. 2025a, *ApJ*, 983, 60
- Chen, K., Li, Z., Inayoshi, K., & Ho, L. C. 2025b, *ApJ*, 994, L42
- Cloonan, A. P., Whitaker, K. E., Manning, S. M., et al. 2026, arXiv e-prints, arXiv:2603.24700
- de Graaff, A., Brammer, G., Weibel, A., et al. 2025a, *A&A*, 697, A189
- de Graaff, A., Hviding, R. E., Naidu, R. P., et al. 2025b, arXiv e-prints, arXiv:2511.21820, submitted to *MNRAS*
- de Graaff, A., Rix, H.-W., Naidu, R. P., et al. 2025c, *A&A*, 701, A168
- D'Eugenio, F., Maiolino, R., Perna, M., et al. 2025, arXiv e-prints, arXiv:2503.11752, published in *MNRAS*
- Ferland, G. J., Chatzikos, M., Guzmán, F., et al. 2017, *Rev. Mexicana Astron. Astrofis.*, 53, 385
- Ferrara, A. 2024, *A&A*, 684, A207
- Furtak, L. J., Secunda, A. R., Greene, J. E., et al. 2025, *A&A*, 698, A227
- Gordon, K. D., Clayton, G. C., Misselt, K. A., Landolt, A. U., & Wolff, M. J. 2003, *ApJ*, 594, 279
- Greene, J. E. & Ho, L. C. 2005, *ApJ*, 630, 122
- Greene, J. E., Labbe, I., Goulding, A. D., et al. 2024, *ApJ*, 964, 39
- Guia, C. A., Pacucci, F., & Kocevski, D. D. 2024, *Research Notes of the American Astronomical Society*, 8, 207
- Hviding, R. E., de Graaff, A., Miller, T. B., et al. 2025, *A&A*, 702, A57
- Inayoshi, K. 2025, *ApJ*, 988, L22
- Inayoshi, K. & Maiolino, R. 2025, *ApJ*, 980, L27
- Inayoshi, K., Murase, K., & Kashiyama, K. 2026, *ApJ*, 1000, 90
- Inayoshi, K., Shanguan, J., Chen, X., Ho, L. C., & Haiman, Z. 2025, arXiv e-prints, arXiv:2505.05322, submitted to *ApJ*
- Jakobsen, P., Ferruit, P., Alves de Oliveira, C., et al. 2022, *A&A*, 661, A80
- Ji, X., D'Eugenio, F., Juodžbalis, I., et al. 2026, *MNRAS*, 545, staf2235
- Ji, X., Maiolino, R., Übler, H., et al. 2025, *MNRAS*, 544, 3900
- Jones, G. C., Übler, H., Maiolino, R., et al. 2026, *MNRAS*, 546, stag115
- Juodžbalis, I., Ji, X., Maiolino, R., et al. 2024, *MNRAS*, 535, 853
- Juodžbalis, I., Marconcini, C., D'Eugenio, F., et al. 2025, arXiv e-prints, arXiv:2508.21748
- Kennicutt, Jr., R. C. 1998, *ARA&A*, 36, 189
- Kido, D., Ioka, K., Hotokezaka, K., Inayoshi, K., & Irwin, C. M. 2025, *MNRAS*, 544, 3407
- Kocevski, D. D., Finkelstein, S. L., Barro, G., et al. 2025, *ApJ*, 986, 126
- Kokubo, M. & Harikane, Y. 2025, *ApJ*, 995, 24
- Korber, D., Marques-Chaves, R., Schaerer, D., et al. 2026, arXiv e-prints, arXiv:2604.08687
- Labbe, I., Greene, J. E., Bezanson, R., et al. 2025, *ApJ*, 978, 92
- Labbe, I., Greene, J. E., Matthee, J., et al. 2024, arXiv e-prints, arXiv:2412.04557, submitted to *ApJ*
- Labbé, I., van Dokkum, P., Nelson, E., et al. 2023, *Nature*, 616, 266
- Leja, J., Carnall, A. C., Johnson, B. D., Conroy, C., & Speagle, J. S. 2019, *ApJ*, 876, 3
- Li, W., Inayoshi, K., Onoue, M., & Toyouchi, D. 2023, *ApJ*, 950, 85
- Lin, R., Zheng, Z.-Y., Jiang, C., et al. 2025, *ApJ*, 980, L34
- Lin, X., Fan, X., Cai, Z., et al. 2026a, *ApJ*, 997, 364
- Lin, X., Fan, X., Sun, F., et al. 2026b, *ApJ*, 997, 61
- Lupi, A., Trinca, A., Volonteri, M., Dotti, M., & Mazzucchelli, C. 2024, *A&A*, 689, A128
- Ma, Y., Greene, J. E., Setton, D. J., et al. 2026, *ApJ*, 1000, 59
- Madau, P., Haardt, F., & Dotti, M. 2014, *ApJ*, 784, L38
- Madau, P. & Maiolino, R. 2026, arXiv e-prints, arXiv:2602.22386
- Maiolino, R., Scholtz, J., Curtis-Lake, E., et al. 2024, *A&A*, 691, A145
- Matthee, J., Naidu, R. P., Brammer, G., et al. 2024, *ApJ*, 963, 129
- Matthee, J., Naidu, R. P., Kotiwale, G., et al. 2025, *ApJ*, 988, 246
- Mérida, R. M., Gaspar, G., Asada, Y., et al. 2026a, *A&A*, 707, A212
- Mérida, R. M., Gaspar, G., Sawicki, M., et al. 2025, *A&A*, 698, A317
- Mérida, R. M., Pérez-González, P. G., Sánchez-Blázquez, P., et al. 2023, *ApJ*, 950, 125
- Mérida, R. M., Sawicki, M., Iyer, K. G., et al. 2026b, *A&A*, 707, A5
- Naidu, R. P., Matthee, J., Katz, H., et al. 2025, arXiv e-prints, arXiv:2503.16596, submitted
- Pacucci, F., Ferrara, A., & Kocevski, D. D. 2026, arXiv e-prints, arXiv:2601.14368
- Pérez-González, P. G., Barro, G., Rieke, G. H., et al. 2024, *ApJ*, 968, 4
- Perger, K., Fogasy, J., Frey, S., & Gabányi, K. É. 2025, *A&A*, 693, L2
- Pizzati, E., Hennawi, J. F., Schaye, J., et al. 2025, *MNRAS*, 539, 2910
- Quadri, G., Trinca, A., Lupi, A., Colpi, M., & Volonteri, M. 2025, *A&A*, 704, A248
- Reines, A. E. & Volonteri, M. 2015, *ApJ*, 813, 82
- Rinaldi, P., Bonaventura, N., Rieke, G. H., et al. 2025, *ApJ*, 992, 71
- Rusakov, V., Watson, D., Nikopoulos, G. P., et al. 2026, *Nature*, 649, 574
- Scholtz, J., D'Eugenio, F., Maiolino, R., et al. 2026, arXiv e-prints, arXiv:2603.22277
- Setton, D. J., Greene, J. E., Spilker, J. S., et al. 2025, *ApJ*, 991, L10
- Shen, X., Hopkins, P. F., Faucher-Giguère, C.-A., et al. 2020, *MNRAS*, 495, 3252
- Sun, W. Q., Naidu, R. P., Matthee, J., et al. 2026, arXiv e-prints, arXiv:2601.20929, submitted to the *Open Journal of Astrophysics*
- Tang, M., Stark, D. P., Plat, A., et al. 2025, *ApJ*, 991, 217
- Taylor, A. J., Kokorev, V., Kocevski, D. D., et al. 2025, *ApJ*, 989, L7
- Torralba, A., Matthee, J., Pezzulli, G., et al. 2026a, *A&A*, 707, A75
- Torralba, A., Matthee, J., Pezzulli, G., et al. 2026b, *A&A*, 705, A147
- Treiber, H., Greene, J. E., Weaver, J. R., et al. 2025, *ApJ*, 984, 93
- Trinca, A., Valiante, R., Schneider, R., et al. 2024, arXiv e-prints, arXiv:2412.14248, submitted to *A&A*
- Tripodi, R., Bradač, M., D'Eugenio, F., et al. 2025a, *ApJ*, 994, L6
- Tripodi, R., Martis, N., Markov, V., et al. 2025b, *Nature Communications*, 16, 9830
- Umeda, H., Inayoshi, K., Harikane, Y., & Murase, K. 2026, *ApJ*, 999, 183
- Wang, B., de Graaff, A., Davies, R. L., et al. 2025, *ApJ*, 984, 121
- Zhang, Z., Jiang, L., Liu, W., & Ho, L. C. 2025, *ApJ*, 985, 119
- Zhuang, M.-Y., Li, J., Shen, Y., et al. 2026, *ApJ*, 999, 31
- Zubovas, K. & King, A. 2021, *MNRAS*, 501, 4289

Appendix A: The effect of the absorption component

Figure A.1 shows a fit to *The Clifff* using the BH*+dust-free host configuration while masking the emission lines and not including the gas absorption component (see Sect. 2 for a detailed description of this feature). The BB model does not fit the data in the vicinity of the break, overestimating the flux and producing an excess clearly reflected in the residuals. *Bagpipes* attributes most of the continuum flux to the BB, eliminating the need for a stellar component. Although not plotted here, the same outcome is observed in the BH*+dusty host configuration.

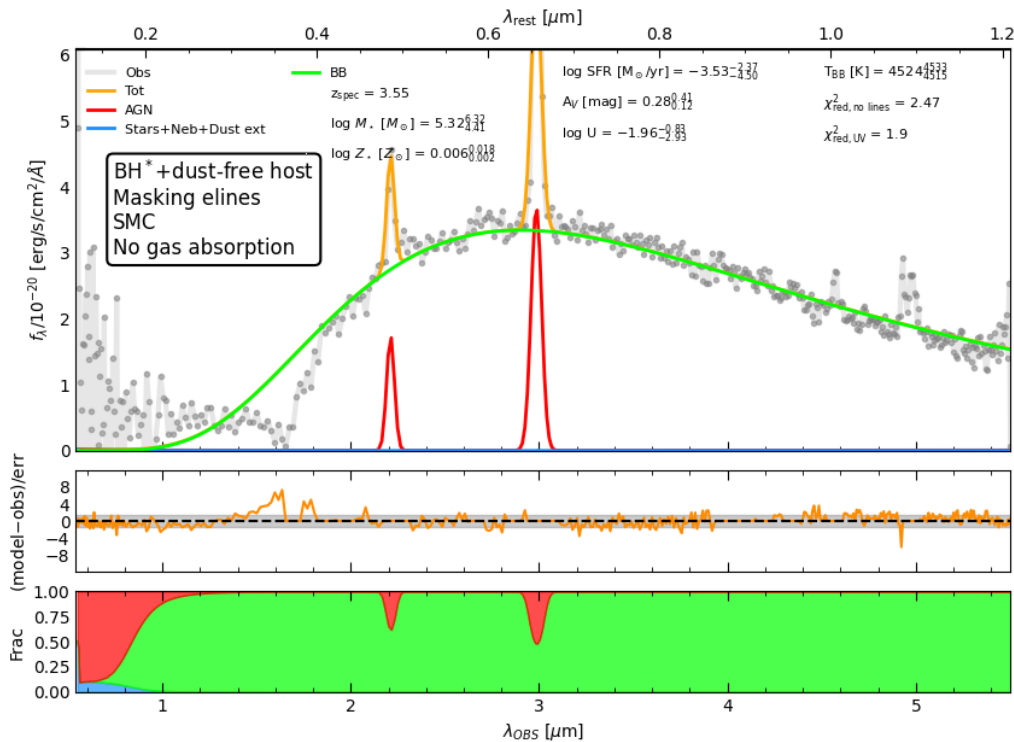


Fig. A.1: Best-fitting model for *The Clifff* using the BH*+dust-free host configuration and an SMC law while masking the emission lines and not including the absorption component. See Fig. 1 for a full description of the markers and color codes shown here. The BB model and the total model overlap in most of the wavelength range. Without this feature, the model overestimates the flux near the Balmer break.

Appendix B: An AGN nature for the UV continuum?

B.1. A host-less scenario

Our model includes stellar, nebular, dust attenuation, AGN, BB, and gas absorption components by construction. Our fits favor a scenario whereby the UV continuum is mostly driven by the host galaxy. In this first section of the appendix, we refitted *The Clifff*'s continuum allowing only an AGN and BB + absorption components. The results are displayed in Figure B.1. 10

The optical continuum is driven by the BB, whereas the UV is powered by the AGN. However, this model underestimates the flux at rest-frame $\lambda > 0.2 \mu\text{m}$, suggesting the need for an additional component.

B.2. The effect of the AGN α_λ slope

In this work, we assumed an AGN model in which the emission from the accretion disk can potentially arise in the UV even with a low AGN normalization factor. In this second section of the appendix, we explore different regimes by narrowing down the α_λ prior, leaving the rest of the priors untouched. We forced an obscured solution by setting $\alpha_\lambda = [0, 2]$, and an unobscured solution by setting $\alpha_\lambda = [-2.8, -1.8]$. In this way, we are changing the effective visibility of the accretion disk. We used the BH*+dusty host configuration and fitted only the continuum, masking the lines.

The best-fitting models from *Bagpipes* obtained with these narrower α_λ priors are displayed in Fig. B.2. The parameters from the Stellar + Nebular models and BB + absorption are consistent with those listed in Table 2. The obscured AGN model yields no AGN contribution to the UV, while the unobscured AGN model leads to some AGN leakage in the UV. These models are statistically indistinguishable, as reflected by their χ^2 values. 20

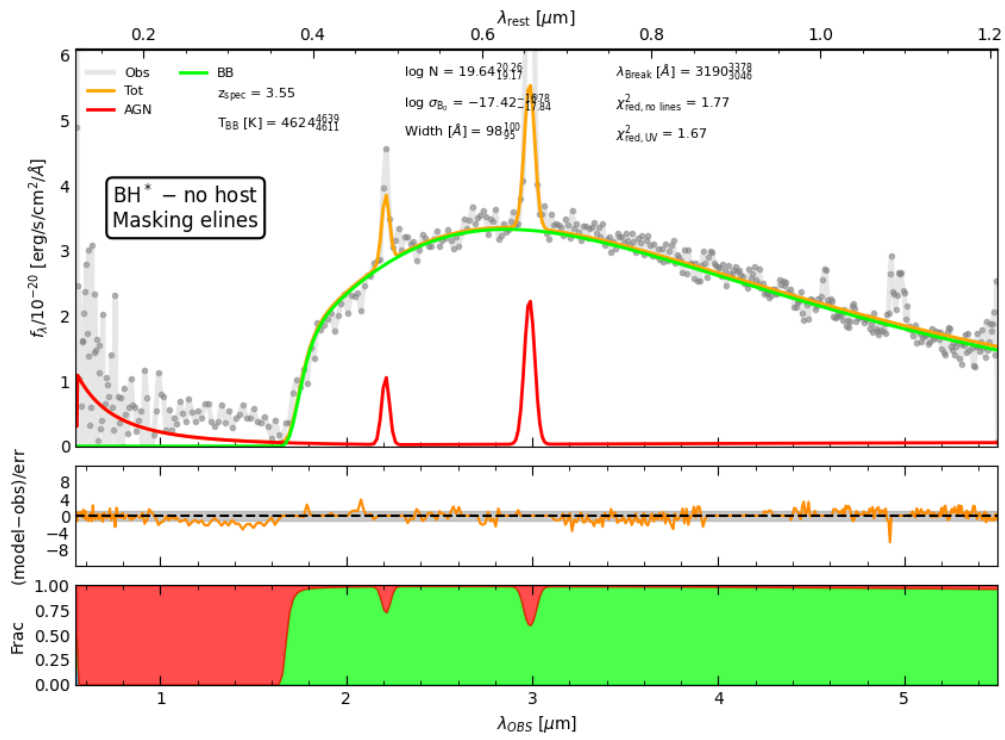
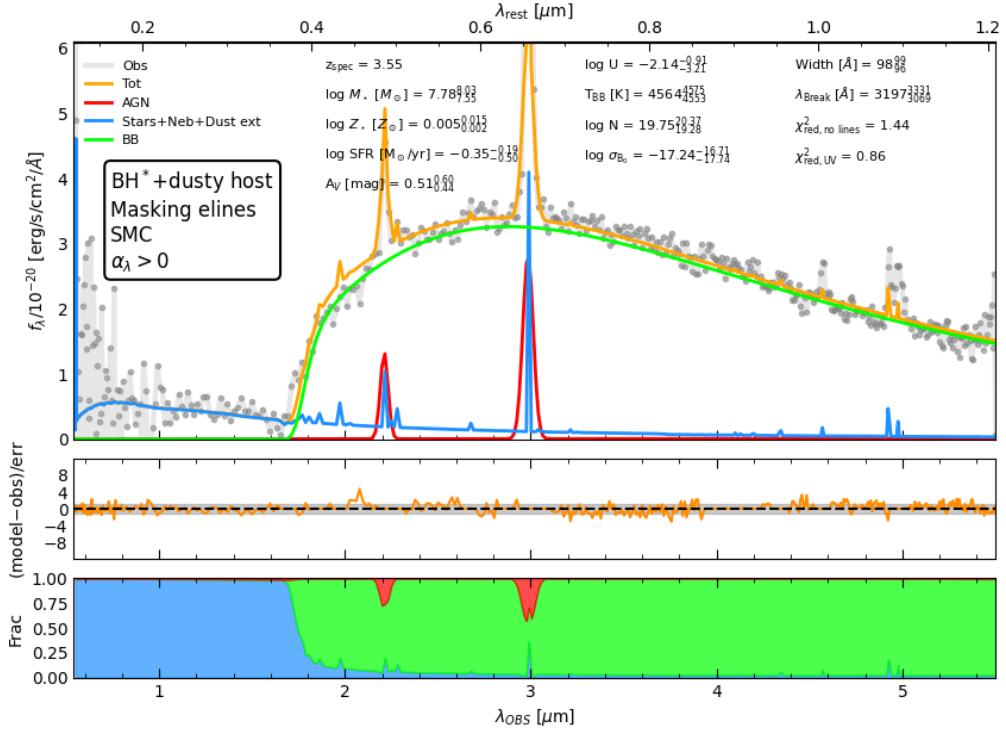
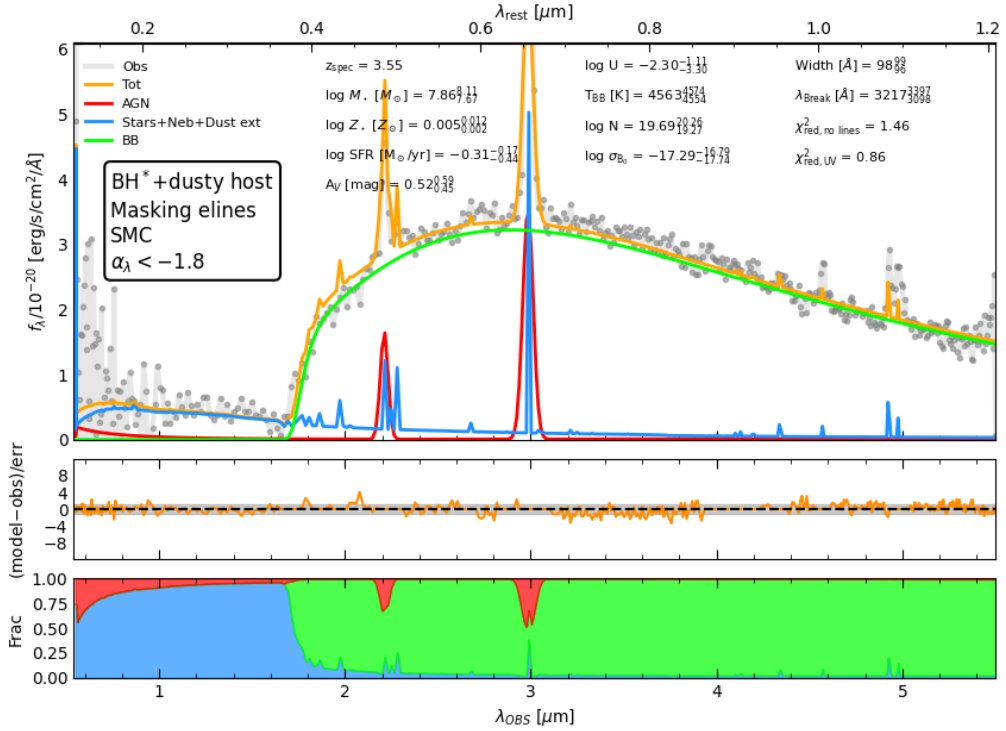


Fig. B.1: Best-fitting model for *The Cliff* masking the emission lines and excluding the stellar, nebular, and dust attenuation components from the fit. See Fig. 1 for a full description of the markers and color codes shown here. The AGN model and the total model overlap in the UV. Without the host galaxy, the model overestimates the flux at rest-frame $\lambda > 0.2 \mu\text{m}$.



(a) SED fitting of *the Cliff* using the BH*+dusty host configuration with an SMC law on the continuum imposing an obscured-AGN model



(b) SED fitting of *the Cliff* using the BH*+dusty host configuration with an SMC law on the continuum imposing an unobscured-AGN model.

Fig. B.2: Best-fitting models from *Bagpipes* using the BH*+dusty host configurations and the continuum emission of *The Cliff*, imposing an obscured AGN (top) and an unobscured AGN (bottom) models. Both are statistically indistinguishable. See Fig. 1 for a full description of the markers and color codes shown here.